ACS APPLIED MATERIALS & INTERFACES

Research Article

www.acsami.org

Ultrathin Dendritic Pt_3Cu Triangular Pyramid Caps with Enhanced Electrocatalytic Activity

Yun Kuang,[†] Zhao Cai,[†] Ying Zhang,[†] Dongsheng He,[§,‡] Xiuling Yan,[∥] Yongmin Bi,[†] Yaping Li,[†] Ziyou Li,*[,‡] and Xiaoming Sun*[,†]

[†]State Key Laboratory of Chemical Resource Engineering, Beijing University of Chemical Technology, Beijing 100029, P. R. China

[‡]Nanoscale Physics Research Laboratory, School of Physics and Astronomy, University of Birmingham, Edgbaston, Birmingham B15 2TT, U.K.

[§]Center of Advanced Nanocatalysis and School of Chemistry and Materials Science, University of Science and Technology of China, Hefei, Anhui 230026, P. R. China

[∥]School of Materials Science and Engineering, Shandong University, Jingshi Road 17923, Ji'nan 250061, P. R. China

Supporting Information

ABSTRACT: Here we report on the synthesis of novel dendritic Pt_3Cu triangular pyramid caps via a solvothermal coreduction method. These caps had three-dimensional caved structures with ultrathin branches, as evidenced by high-resolution transmission electron microscopy (HRTEM) and HAADF-STEM characterization. Tuning the reduction kinetics of two metal precursors by an iodide ion was believed to be the key for the formation of an alloyed nanostructure. Electro-oxidation of methanol and formic acid showed dramatically improved electrocatalytic activities and poison-tolerance for these nanoalloys as compared to commercial Pt/C catalysts, which was attributed to their unique open porous structure with interconnected network, ultrahigh surface areas, as well as synergetic effect of the two metallic components.

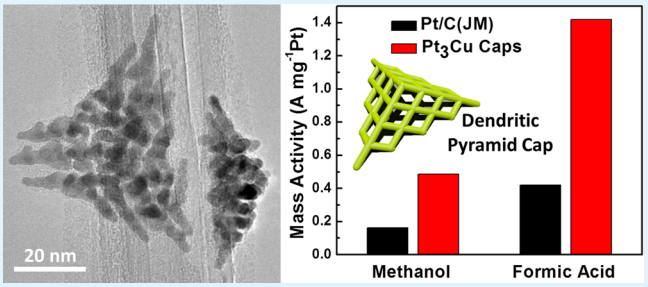

KEYWORDS: *dendritic pyramid cap, Pt_3Cu alloy, ultrathin branch, fuel oxidation, anti-CO poisoning*

INTRODUCTION

Bimetallic alloy nanostructures have been broadly believed to be substitutes for pure noble metal catalysts toward various electrochemical reactions.[1−4] By combining less expensive transition metals with noble metals, such alloy structures not only reduce the use of precious noble metal but also improve the overall performance due to synergetic effects.[5−12]

Recently, shape-controlled synthesis[13−16] of various ultrathin alloyed nanoparticles has been reported to have high intrinsic electrocatalytic activities.[3,9,17−22] However, aggregation and loss of contact with electroconductive supports have greatly limited the practical application of zero-dimensional (0D) nanoparticles. As estimated, only 20−30% was chemically accessible for reactant and connects to an external circuit.[23] Though ultrathin nanowires and nanosheets enhanced electroconductivity and electrocatalytic activity to certain degrees,[24−28] overlap of their accessible sites remained a big issue.

Ideally electrocatalysts should have three-dimensional (3D) open porous but interconnected/integrated networks with ultrahigh surface areas (i.e., ultrathin branches).[29−32] Herein, as a typical Pt-based alloy for a fuel cell cathode,[28,31] we synthesized dendritic Pt_3Cu triangular pyramid caps with integrated ultrathin branches. Compared with commercial Pt/C catalyst, the open porous alloy pyramids showed 3/3.38-fold enhancement on mass activity and 2.14/2.41-fold enhancement on specific activity toward the electrocatalytic methanol/formic acid oxidation and, more importantly, a much higher anti-CO poisoning performance. The combination of the above merits made the dendritic pyramid caps promising for practical applications.

RESULTS AND DISCUSSION

In a typical synthesis of ultrathin PtCu nanostructures, potassium tetrachloroplatinate (K_2PtCl_4), copper dichloride ($CuCl_2$), polyvinylpyrrolidone (PVP), and potassium iodide (KI) were dissolved in a mixed solvent containing water and formamide (FA). The resultant homogeneous solution was then solvothermally treated in a Teflon-lined stainless steel autoclave at 120 °C for 4 h (see Supporting Information for details).

TEM images (Figure 1A−F) show morphology evolution of the as-synthesized PtCu nanostructures. Increasing the molar ratio of Pt/Cu precursors from 1:3 to 3:1, the morphologies changed from tripods to dendritic triangular pyramids, while

Received: June 28, 2014
Accepted: September 29, 2014
Published: September 29, 2014

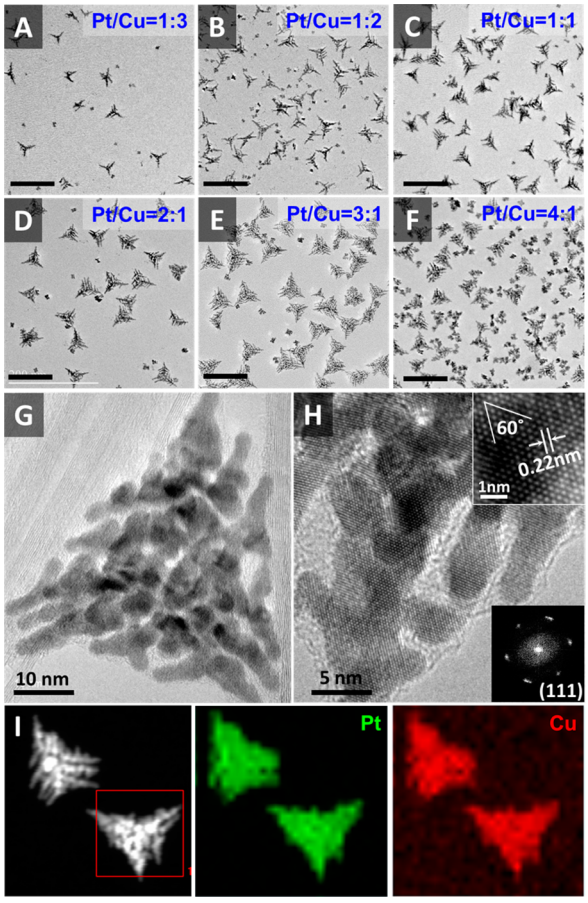

Figure 1. TEM images of morphology evolution for dendritic Pt_3Cu pyramids with different Pt/Cu precursor molar ratios: (A) 1:3, (B) 1:2, (C) 1:1, (D) 2:1, (E) 3:1, and (F) 4:1. (G) and (H) high-resolution transmission electron microscopy (HRTEM) images (inset shows enlarged image and the corresponding fast Fourier transform (FFT) pattern) of a typical dendritic triangular pyramid in (E). (I) HAADF-STEM image with the corresponding spectral mapping of Pt and Cu. Default scale bars are 100 nm.

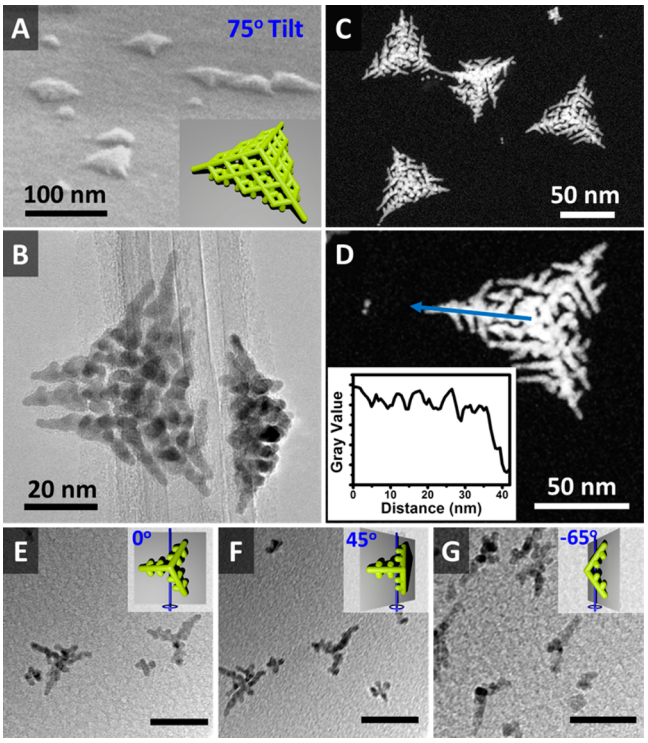

Figure 2. (A) 75° tilting SEM image (inset shows a 3D model) of the pyramids. (B) HRTEM image of dendritic Pt_3Cu triangular pyramids laid on a carbon nanotube supported TEM grid. (C) and (D) HAADF-STEM image (inset shows the line profile) of the pyramids. (E)−(G) Tilted TEM images (inset shows the top view of a 3D model) of a 20 min Pt_3Cu intermediate. Scale bars in (E)−(G) are 30 nm.

further increase of the ratio (Pt:Cu = 4:1) resulted in wider branches and small dendrites. However, without a Cu precursor it only resulted in spherical nanoparticles (Figure S1, Supporting Information). The HRTEM image (Figure 1G) shows a typical dendritic triangular pyramid (Pt:Cu = 3:1), which has a hierarchical branched structure with 3.8 nm width of the branches on average. An enlarged HRTEM image (inset of Figure 1H) of the branches shows that the lattice fringes correspond to a spacing of 0.22 nm, which matches the *d* spacing of the (111) plane of the Pt_3Cu alloy.[28,31] EDS mapping of the dendritic alloys shows that Pt and Cu atoms are uniformly distributed with an atomic ratio of 75.6% and 24.4%, respectively. Inductively coupled plasma optical emission spectrometry (ICP-OES) was also applied for composition investigation, and the result suggested a Pt/Cu atomic ratio of ~3:1 (76:24), which was almost the same as EDS data, demonstrating the compositional homogeneity of the dendritic particles. The X-ray diffraction (XRD, Figure S2, Supporting Information) pattern of the dendritic Pt_3Cu pyramids displays characteristic peaks that are in agreement with those of a well-crystallized Pt pattern with face-centered-cubic (fcc) structure (JCPDS No. 65-2868) but show a little shift to higher angle, confirming an alloyed structure.[33]

Interestingly, the dendritic triangular pyramids had a "cave" at the center of the 3D porous structures, which made it "cap-like" as revealed by morphology and structure characterization (Figure 2). Scanning electron microscopy (SEM, Figure 2A, taken at 75° tilting substrate) images clearly evidenced a nonplanar triangular pyramid structure of the final products. Two individual pyramids laid on a carbon nanotube supported TEM grid, one top view and the other side view (bottom facet of pyramid "vertical" and "parallel" to the electron beam), were typically shown in Figure 2B. The angle ~112° in the side-view image unambiguously evidenced the pyramid structure. The hollow cave structure is evidenced by a thickness-sensitive high-angle annular dark-field scanning transmission electron microscopy (HAADF-STEM, Figure 2C and 2D) analysis:[34] the line profile along the ridge of the individual pyramid (the blue arrow in Figure 2D), which shows almost the constant intensity from the center to the edge. This suggests the ridge has a constant thickness without accumulated growth at the center, demonstrating a "cave" structure. Another vertical-laid less grown pyramid with one ridge perpendicular to the paper (Figure S3, Supporting Information) confirmed the cap-like structure of the pyramids by showing two opened legs. Tilted TEM microscopy (Figure 2E−G) of two tripod intermediates (20 min reaction) reveals the exact spatial location of the three ridges/legs. A tripod structure with 120° intersection angles was seen in the top-view image (Figure 2E). Two of the three legs made an almost straight line as the sample was tilted +45° (Figure 2F). In contrast, one of the legs shrank to a dark dot

dx.doi.org/10.1021/am5041412 | ACS Appl. Mater. Interfaces 2014, 6, 17748−17752

(Figure 2G) when the sample stage was tilted to −65°, suggesting the leg was parallel to the electron beam. The cartoon models were schemed in the insets.

The key factor for the formation of alloyed structure was believed to be I^- ions, which tune the reduction kinetics of the two precursors by coordinating with Pt^{II} to form a more stable PtI_4^{2-} (PtI_4^{2-}/Pt, E = 0.32 V;[35,36] $PtCl_4^{2-}$/Pt, E = 0.758 V) and at the same time reducing Cu^{II} to Cu^{I} species, which is easy to be further reduced to Cu^0 (Cu^+/Cu, E = 0.52 V, Cu^{2+}/Cu, E = 0.34 V). Besides, disproportionation reaction on CuI would automatically occur and thus release Cu^0 slowly even without any reducing reagent. It seems that the reduction of Cu^{II} and Pt^{II} occurred almost simultaneously, forming alloyed nuclei as indicated in the STEM image of a captured primary seed formed at the initial stage (5 min, Figure 3A). However, without KI or replacing KI with KCl or KBr only resulted in heterostructures (Figure S4, Supporting Information).

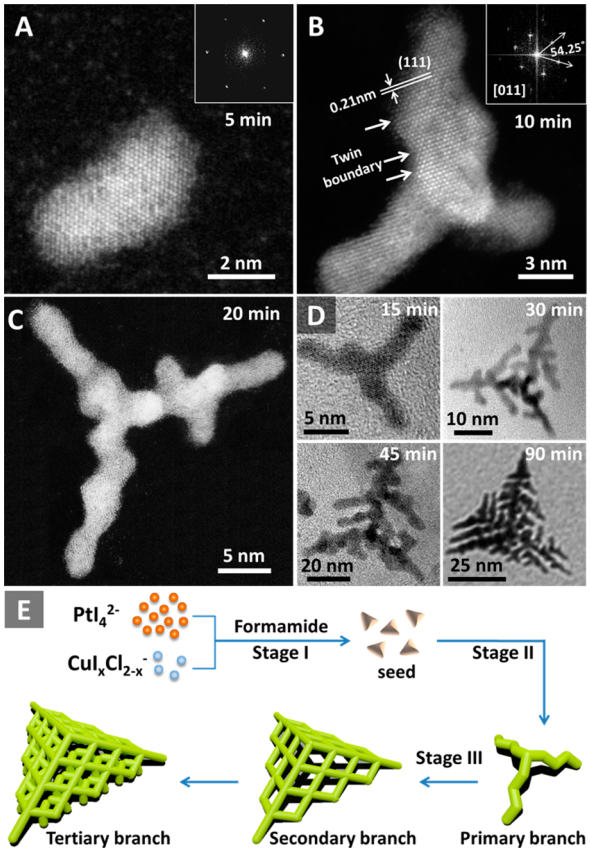

Figure 3. STEM images of (A) a captured primary particle and (B) a primary tripod. (C) STEM tomography of the 20 min intermediate. (D) TEM images of the intermediates of Pt_3Cu triangular pyramids at different reaction time point. (E) Schematic illustration of the formation process of the dendritic Pt_3Cu triangular pyramids.

In order to reveal the formation process of the dendritic triangular pyramid caps, time-dependent structure evolution reaction was carried out. Morphology evolution shown in both TEM images (Figure 3A–D) and schematic illustration (Figure 3E) reveal three formation stages of dendritic triangular pyramid caps: first, the primary seeds are formed within 5 min of reaction time (Figure 3A); second the formation and elongation of the primary tripod backbone occurred before 20 min (Figure 3B and 3C); and finally the branches are formed along with further elongation of the backbone (Figure 3D).

It is believed that rich structural defects induced by Cu doping played a key role in the formation of hierarchical structures. Inhomogeneous growth at the defect-enriched region of a primary seed led to the formation of primary tripods (i.e., ridges), which coincided with a previous report.[37] Furthermore, defects would induce much stacking faults, as could be seen from the twin boundaries (Figure 3B), which made the backbones show an obvious zigzag pattern (Figure 3C). The growth modes were repeated at the convex sites and led to new branch formation, possibly because these sites were relatively more active, and galvanic reaction between Pt^{II} and Cu^0 could happen therein. The HAADF-STEM image of the 20 min intermediate (Figure 3C) clearly confirms that the formation of the secondary branch started on the convex sites of the backbone. As-formed branches grew parallel to the neighboring ridges or primary branches possibly for minimizing the lattice mismatch.

The relative complex formation procedure made the structure very sensitive to the synthetic parameters. Besides the Pt/Cu precursor ratio mentioned before, variations of KI amount (Figure S4, Supporting Information), solvent species (Figure S5, Supporting Information), water/formamide ratio (Figure S6, Supporting Information), and metal precursor species (Figure S7, Supporting Information) all would weaken the dendritic structure and reduce the amount of branches, or even eliminate the branched structures. It is believed that the low solubility or low coordination ability of I^- in such a reaction environment weakened reduction kinetic control of the two metal precursors.

The as-prepared Pt_3Cu triangular pyramid caps showed superior electrochemical properties on electro-oxidations of methanol and formic acid alloy than commercial Pt/C electrocatalyst (Johnson Matthey, JM 40 wt %). Cyclic voltammetry (CV, Figure 4A) and CO stripping (Figure S8, Supporting Information) were used to evaluate the electrochemically active surface area (ECSA) of the Pt_3Cu triangular pyramid caps and commercial Pt/C catalysts. Calculated from CO-adsorption charge, the Pt_3Cu triangular pyramid caps showed a high ECSA of 68.3 m^2/g, which is much higher than that of a commercial Pt/C (48.4 m^2/g) catalyst.

We further investigated the electrocatalytic oxidation of small fuel molecules (methanol and formic acid) on the dendritic Pt_3Cu triangular pyramid caps and commercial Pt/C electrocatalyst. In order to compare the activity, the currents were normalized with respect to both the electrochemically active surface area and the loading amount of Pt (Figures S9 and S10, Supporting Information). Comparison of specific activities and mass activities between dendritic Pt_3Cu triangular pyramids and commercial Pt/C catalyst are shown in Figure 4B and 4C. The specific activity of the Pt_3Cu pyramid cap is 2.04- and 2.41-fold of the Pt/C catalyst, while the mass activity is 3- and 3.38-fold of Pt/C for methanol and formic acid electro-oxidation, respectively. The enhanced specific and mass activity for the Pt_3Cu pyramid caps may be ascribed to its unique ultrathin, hollow, and three-dimensional open porous structure together with high ECSA and interconnected network. Chronoamperometric (CA) measurements performed at 0.9 V (Figure 4E) further confirmed the the Pt_3Cu pyramid cap had a higher current density as well as higher stability than the Pt/C catalyst. TEM images of the Pt_3Cu pyramid caps after 50 cycles of CV treatment (Figure S11B, Supporting Information) and

dx.doi.org/10.1021/am5041412 | ACS Appl. Mater. Interfaces 2014, 6, 17748−17752

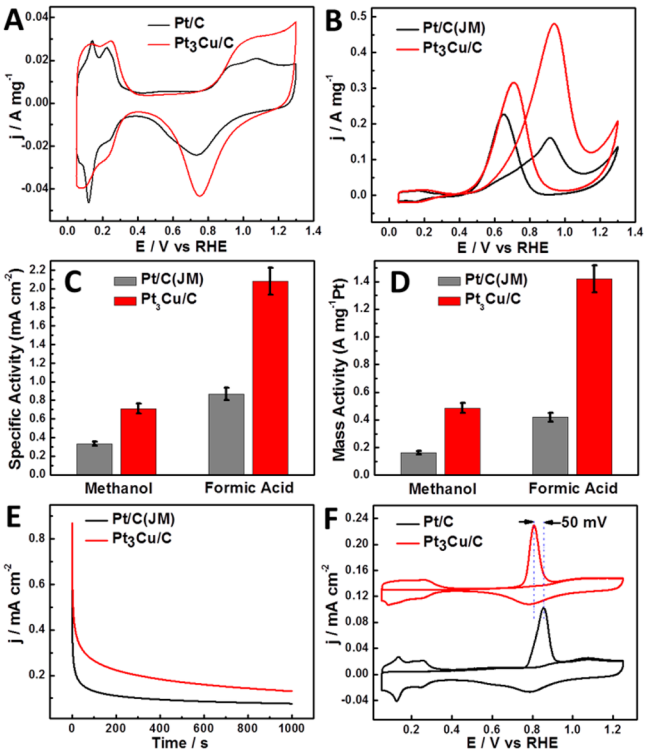

Figure 4. Mass normalized CV curves of Pt/C (JM, 40 wt %) and dendritic Pt_3Cu triangular pyramids/C in (A) 0.5 M H_2SO_4 (scan rate: 20 mV/s) and (B) 0.5 M H_2SO_4 + 1 M MeOH (scan rate: 50 mV/s). (C) Specific activities and (D) mass activities of Pt_3Cu triangular pyramids and Pt/C on methanol and formic acid electro-oxidation. (E) Chronoamperometric (CA) measurement (in 0.5 M H_2SO_4 + 1 M MeOH solution, at 0.9 V vs RHE) and (F) CO stripping of the two catalysts.

chronoamperometry test (Figure S11C, Supporting Information) also revealed that the Pt_3Cu pyramid caps showed high stability after the electrochemical durability test.

Besides high current density, the dendritic Pt_3Cu triangular pyramid cap also showed a high anti-CO poisoning performance toward both methanol and formic acid oxidation reaction. For the methanol oxidation reaction (MOR), the Pt_3Cu pyramid cap exhibited a high I_f/I_b = 1.55 ratio, in which I_f and I_b are the forward and backward current densities, respectively (Figure 4B), which was 2.06 times of the Pt/C catalyst (I_f/I_b = 0.76), implying that methanol molecules mainly go through a direct oxidation pathway on the Pt_3Cu pyramids, thus generating relatively less poisoning species as compared to the Pt/C electrocatalyst.[38] The CO-stripping peak of dendritic Pt_3Cu pyramid caps shifted 50 mV to lower potential, indicating a weaker Pt−CO bond strength compared to that of Pt/C. This result was consistent with the calculation of CO-adsorption energies obtained from DFT simulation, which are −1.46 and −1.26 eV for the Pt and Pt_3Cu surface, respectively (see Supporting Information for calculation details). On the other hand, for the indirect pathway, H_2O must be involved in the CO oxidation reaction in the acidic environment. Pt could readily oxidize methanol to CO but has difficulty in oxidizing CO to CO_2, owing to its strong binding to OH and poor ability to activate water. However, the alloy of Cu could lower the binding energy for both CO and OH adsorption, and thus, forming the Pt−Cu alloy could accelerate the oxidation of CO.[39] Therefore, combining the above reasons, the dendritic Pt_3Cu pyramid caps show relatively high anti-CO poisoning performance.

CONCLUSIONS

In summary, ultrathin dendritic Pt_3Cu triangular pyramid caps have been synthesized through a solvothermal coreduction method tuned by iodide ion coordination. The as-synthesized dendritic Pt_3Cu triangular pyramid caps showed excellent electrocatalytic activity and anti-CO poisoning performance, demonstrating the great potential of the dendritic ultrathin alloy structure for constructing an advanced electrocatalyst due to their tailored synergetic effects, fully exposed active sites, and integrated conductive structure. This result demonstrates the importance for constructing open porous interconnected nanostructures for electrocatalysis and also provides opportunities to design and fabricate other ultrathin dendritic bimetallic structures by tailored growth kinetics, which would be of great importance in the field of clean energy and green chemistry.

ASSOCIATED CONTENT

Supporting Information

Experimental details, supplementary TEM, SEM, STEM figures, and electrochemical measurements. This material is available free of charge via the Internet at http://pubs.acs.org.

AUTHOR INFORMATION

Corresponding Authors

*E-mail: sunxm@mail.buct.edu.cn.
*E-mail: z.li@bham.ac.uk.

Notes

The authors declare no competing financial interest.

ACKNOWLEDGMENTS

The authors thank Dr. Yu-Lung Chiu and Z. Liu for the technical assistance on tilted TEM microscopy and D.X. Yang on SEM. The work in China was supported by National Natural Science Foundation of China, the 863 Program (2012AA03A609) and 973 Program (2011CBA00503, 2011CB932403, 2012CB932800). The work in UK was supported by EPSRC (EP/G070326/1). ZYL acknowledges the support from COST Action MP0903.

REFERENCES

(1) Wang, D.; Li, Y. Bimetallic Nanocrystals: Liquid-Phase Synthesis and Catalytic Applications. *Adv. Mater.* **2011**, *23*, 1044−1060.

(2) Lim, B.; Jiang, M.; Camargo, P. H. C.; Cho, E. C.; Tao, J.; Lu, X.; Zhu, Y.; Xia, Y. Pd-Pt Bimetallic Nanodendrites with High Activity for Oxygen Reduction. *Science* **2009**, *324*, 1302−1305.

(3) Wang, D.; Xin, H. L.; Hovden, R.; Wang, H.; Yu, Y.; Muller, D. A.; DiSalvo, F. J.; Abruña, H. D. Structurally ordered intermetallic platinum−cobalt core−shell nanoparticles with enhanced activity and stability as oxygen reduction electrocatalysts. *Nat. Mater.* **2013**, *12*, 81−87.

(4) Strmcnik, D.; Uchimura, M.; Wang, C.; Subbaraman, R.; Danilovic, N.; van der, V.; Paulikas, A. P.; Stamenkovic, V. R.; Markovic, N. M. Improving the hydrogen oxidation reaction rate by promotion of hydroxyl adsorption. *Nat. Chem.* **2013**, *5*, 300−306.

(5) Stamenkovic, V. R.; Mun, B. S.; Arenz, M.; Mayrhofer, K. J. J.; Lucas, C. A.; Wang, G.; Ross, P. N.; Markovic, N. M. Trends in electrocatalysis on extended and nanoscale Pt-bimetallic alloy surfaces. *Nat. Mater.* **2007**, *6*, 241−247.

(6) Greeley, J.; Stephens, I. E. L.; Bondarenko, A. S.; Johansson, T. P.; Hansen, H. A.; Jaramillo, T. F.; Rossmeisl, J.; Chorkendorff, I.;

Nørskov, J. K. Alloys of platinum and early transition metals as oxygen reduction electrocatalysts. *Nat. Chem.* **2009**, *1*, 552−556.
(7) Mu, R.; Fu, Q.; Xu, H.; Zhang, H.; Huang, Y.; Jiang, Z.; Zhang, S.; Tan, D.; Bao, X. Synergetic Effect of Surface and Subsurface Ni Species at Pt−Ni Bimetallic Catalysts for CO Oxidation. *J. Am. Chem. Soc.* **2011**, *133*, 1978−1986.
(8) Wang, Y.; Chen, G.; Yang, M.; Silber, G.; Xing, S.; Tan, L. H.; Wang, F.; Feng, Y.; Liu, X.; Li, S.; Chen, H. A systems approach towards the stoichiometry-controlled hetero-assembly of nanoparticles. *Nat. Commun.* **2010**, *1*, 87.
(9) Huang, X.; Zhu, E.; Chen, Y.; Li, Y.; Chiu, C.-Y.; Xu, Y.; Lin, Z.; Duan, X.; Huang, Y. A Facile Strategy to Pt3Ni Nanocrystals with Highly Porous Features as an Enhanced Oxygen Reduction Reaction Catalyst. *Adv. Mater.* **2013**, *25*, 2974−2979.
(10) Xu, D.; Liu, Z.; Yang, H.; Liu, Q.; Zhang, J.; Fang, J.; Zou, S.; Sun, K. Solution-Based Evolution and Enhanced Methanol Oxidation Activity of Monodisperse Platinum−Copper Nanocubes. *Angew. Chem., Int. Ed.* **2009**, *48*, 4217−4221.
(11) Guo, S.; Zhang, S.; Sun, S. Tuning Nanoparticle Catalysis for the Oxygen Reduction Reaction. *Angew. Chem., Int. Ed.* **2013**, *52*, 8526−8544.
(12) Siriwatcharapiboon, W.; Kwon, Y.; Yang, J.; Chantry, R. L.; Li, Z.; Horswell, S. L.; Koper, M. T. M. Promotion Effects of Sn on the Electrocatalytic Reduction of Nitrate at Rh Nanoparticles. *Chem. Electrochem.* **2014**, *1*, 172−179.
(13) Xia, Y.; Xiong, Y.; Lim, B.; Skrabalak, S. E. Shape-Controlled Synthesis of Metal Nanocrystals: Simple Chemistry Meets Complex Physics? *Angew. Chem., Int. Ed.* **2009**, *48*, 60−103.
(14) Gumeci, C.; Marathe, A.; Behrens, R. L.; Chaudhuri, J.; Korzeniewski, C. Solvothermal Synthesis and Electrochemical Characterization of Shape-Controlled Pt Nanocrystals. *J. Phys. Chem. C* **2014**, *118*, 14433−14440.
(15) Fennell, J.; He, D.; Tanyi, A. M.; Logsdail, A. J.; Johnston, R. L.; Li, Z. Y.; Horswell, S. L. A Selective Blocking Method To Control the Overgrowth of Pt on Au Nanorods. *J. Am. Chem. Soc.* **2013**, *135*, 6554−6561.
(16) Chantry, R. L.; Siriwatcharapiboon, W.; Horswell, S. L.; Logsdail, A. J.; Johnston, R. L.; Li, Z. Y. Overgrowth of Rhodium on Gold Nanorods. *J. Phys. Chem. C* **2012**, *116*, 10312−10317.
(17) Xu, C.; Wang, L.; Wang, R.; Wang, K.; Zhang, Y.; Tian, F.; Ding, Y. Nanotubular Mesoporous Bimetallic Nanostructures with Enhanced Electrocatalytic Performance. *Adv. Mater.* **2009**, *21*, 2165−2169.
(18) Guo, S.; Sun, S. FePt Nanoparticles Assembled on Graphene as Enhanced Catalyst for Oxygen Reduction Reaction. *J. Am. Chem. Soc.* **2012**, *134*, 2492−2495.
(19) Zhang, J.; Fang, J. A General Strategy for Preparation of Pt 3d-Transition Metal (Co, Fe, Ni) Nanocubes. *J. Am. Chem. Soc.* **2009**, *131*, 18543−18547.
(20) Kang, Y.; Murray, C. B. Synthesis and Electrocatalytic Properties of Cubic Mn−Pt Nanocrystals (Nanocubes). *J. Am. Chem. Soc.* **2010**, *132*, 7568−7569.
(21) Xu, D.; Bliznakov, S.; Liu, Z.; Fang, J.; Dimitrov, N. Composition-Dependent Electrocatalytic Activity of Pt-Cu Nanocube Catalysts for Formic Acid Oxidation. *Angew. Chem., Int. Ed.* **2010**, *122*, 1304−1307.
(22) Zhu, C.; Guo, S.; Dong, S. PdM (M = Pt, Au) Bimetallic Alloy Nanowires with Enhanced Electrocatalytic Activity for Electrooxidation of Small Molecules. *Adv. Mater.* **2012**, *24*, 2326−2331.
(23) Wang, C.; Waje, M.; Wang, X.; Tang, J. M.; Haddon, R. C. Yan, Proton Exchange Membrane Fuel Cells with Carbon Nanotube Based Electrodes. *Nano Lett.* **2003**, *4*, 345−348.
(24) Guo, S.; Li, D.; Zhu, H.; Zhang, S.; Markovic, N. M.; Stamenkovic, V. R.; Sun, S. FePt and CoPt Nanowires as Efficient Catalysts for the Oxygen Reduction Reaction. *Angew. Chem., Int. Ed.* **2013**, *125*, 3549−3552.
(25) Yang, S.; Hong, F.; Wang, L.; Guo, S.; Song, X.; Ding, B.; Yang, Z. Ultrathin Pt-Based Alloy Nanowire Networks: Synthesized by CTAB Assistant Two-Phase Water−Chloroform Micelles. *J. Phys. Chem. C* **2009**, *114*, 203−207.
(26) Liang, H.-W.; Cao, X.; Zhou, F.; Cui, C.-H.; Zhang, W.-J.; Yu, S.-H. A Free-Standing Pt-Nanowire Membrane as a Highly Stable Electrocatalyst for the Oxygen Reduction Reaction. *Adv. Mater.* **2011**, *23*, 1467−1471.
(27) Xia, B. Y.; Wu, H. B.; Yan, Y.; Lou, X. W.; Wang, X. Ultrathin and Ultralong Single-Crystal Platinum Nanowire Assemblies with Highly Stable Electrocatalytic Activity. *J. Am. Chem. Soc.* **2013**, *135*, 9480−9485.
(28) Saleem, F.; Zhang, Z.; Xu, B.; Xu, X.; He, P.; Wang, X. Ultrathin Pt−Cu Nanosheets and Nanocones. *J. Am. Chem. Soc.* **2013**, *135*, 18304−18307.
(29) Chen, C.; Kang, Y.; Huo, Z.; Zhu, Z.; Huang, W.; Xin, H. L.; Snyder, J. D.; Li, D.; Herron, J. A.; Mavrikakis, M.; Chi, M.; More, K. L.; Li, Y.; Markovic, N. M.; Somorjai, G. A.; Yang, P.; Stamenkovic, V. R. Highly Crystalline Multimetallic Nanoframes with Three-Dimensional Electrocatalytic Surfaces. *Science* **2014**, *343*, 1339−1343.
(30) Lim, B.; Xia, Y. Metal Nanocrystals with Highly Branched Morphologies. *Angew. Chem., Int. Ed.* **2011**, *50*, 76−85.
(31) Ma, L.; Wang, C.; Gong, M.; Liao, L.; Long, R.; Wang, J.; Wu, D.; Zhong, W.; Kim, M. J.; Chen, Y.; Xie, Y.; Xiong, Y. Control Over the Branched Structures of Platinum Nanocrystals for Electrocatalytic Applications. *ACS Nano* **2012**, *6*, 9797−9806.
(32) Huang, X.; Zhang, H.; Guo, C.; Zhou, Z.; Zheng, N. Simplifying the Creation of Hollow Metallic Nanostructures: One-Pot Synthesis of Hollow Palladium/Platinum Single-Crystalline Nanocubes. *Angew. Chem., Int. Ed.* **2009**, *121*, 4902−4906.
(33) Tseng, Y.-C.; Chen, H.-S.; Liu, C.-W.; Yeh, T.-H.; Wang, K.-W. The effect of alloying on the oxygen reduction reaction activity of carbon-supported PtCu and PtPd nanorods. *J. Mater. Chem. A* **2014**, *2*, 4270−4275.
(34) Li, Z. Scanning Transmission Electron Microscopy Studies of Mono-and Bi-metallic Nanoclusters. In *Metal Nanoparticles and Alloys*, 3rd ed.; Roy Luigi Johnston, J. P. W., Ed.; Elsevier: Amsterdam, 2012; Vol. 3, pp 213−245.
(35) Nagahara, Y.; Hara, M.; Yoshimoto, S.; Inukai, J.; Yau, S.-L.; Itaya, K. In Situ Scanning Tunneling Microscopy Examination of Molecular Adlayers of Haloplatinate Complexes and Electrochemically Produced Platinum Nanoparticles on Au(111). *J. Phys. Chem. B* **2004**, *108*, 3224−3230.
(36) Dawson, R. J.; Kelsall, G. H. Pt Dissolution and Deposition in High Concentration Aqueous Tri-Iodide/Iodide Solutions. *ECS Electrochem. Lett.* **2013**, *2*, 55−57.
(37) Maksimuk, S.; Teng, X.; Yang, H. Roles of Twin Defects in the Formation of Platinum Multipod Nanocrystals. *J. Phys. Chem. C* **2007**, *111*, 14312−14319.
(38) Housmans, T. H. M.; Wonders, A. H.; Koper, M. T. M. Structure Sensitivity of Methanol Electrooxidation Pathways on Platinum: An On-Line Electrochemical Mass Spectrometry Study. *J. Phys. Chem. B* **2006**, *110*, 10021−10031.
(39) Tritsaris, G. A.; Rossmeisl, J. Methanol Oxidation on Model Elemental and Bimetallic Transition Metal Surfaces. *J. Phys. Chem. C* **2012**, *116*, 11980−11986.